Int J Fract (2012) 173:91–104
DOI 10.1007/s10704-011-9666-y

ORIGINAL PAPER

A cohesive crack model coupled with damage for interface fatigue problems

Baoming Gong · Marco Paggi · Alberto Carpinteri

Received: 11 May 2011 / Accepted: 15 December 2011 / Published online: 20 January 2012

Abstract An semi-analytical formulation based on the cohesive crack model is proposed to describe the phenomenon of fatigue crack growth along an interface. Since the process of material separation under cyclic loading is physically governed by cumulative damage, the material deterioration due to fatigue is taken into account in terms of interfacial cohesive properties degradation. More specifically, the damage increment is determined by the current separation and a history variable. The damage variable is introduced into the constitutive cohesive crack law in order to capture the history-dependent property of fatigue. Parametric studies are presented to understand the influences of the two parameters entering the damage evolution law. An application to a pre-cracked double-cantilever beam is discussed. The model is validated by experimental data. Finally, the effect of using different shapes of the cohesive crack law is illustrated

Keywords Cohesive crack model · Fatigue damage · Interface · Double cantilever beam

B. Gong (✉) · M. Paggi · A. Carpinteri
Department of Structural Engineering and Geotechnics, Politecnico di Torino, Corso Duca degli Abruzzi 24, 10129, Torino, Italy
e-mail: baoming.gong@polito.it

M. Paggi
e-mail: marco.paggi@polito.it

A. Carpinteri
e-mail: alberto.carpinteri@polito.it

1 Introduction

Components with interfaces subjected to cyclic loading are widely used in engineering and their fatigue failure is inevitable. Due to the complexity of fatigue failure, the predictions of crack growth rate and fatigue life are still challenging tasks. In general, both fracture mechanics and damage mechanics are conventionally used to capture the fatigue phenomena.

The application of fracture mechanics in fatigue can be traced back to the pioneering work by Paris et al. (1961), who related the crack growth rate, $\mathrm{d}a/\mathrm{d}N$, to the applied stress-intensity factor range, ΔK. Since then, several alternative methods have been proposed in terms of J-integral range, ΔJ, crack tip opening displacement variation, Δ CTOD, or strain energy release rate range, ΔG, (Dowling and Begley 1976; Neumann 1974; Mostovoy and Ripling 1975; Hertzberg 1995) to extend the application of Paris' law. It is worth noting that the latter has been frequently employed by several authors to investigate the problem of interface crack growth (Roe and Siegmund 2003; Pirondi and Nicoletto 2004; Maiti and Geubelle 2005, 2006; Carpinteri et al. 2008).

Fatigue and fracture problems can also be tackled using Damage Mechanics, which is also recently incorporated into nonlinear fracture models to capture finite life effects by several researchers. Kachanov (1958) firstly modelled the loss of stiffness due to microcracks and their effect on the integrity of components using a macroscopic damage parameter depending on

the density of microcracks. Regarding fatigue damage, Chaboche and Lesne (1988) established a model known as *Nonlinear Continuous Damage*, which postulates a fatigue damage increment per cycle dependent on the stress state and on the current damage level. Lemaitre and Plumtree (1979), Wang (1992), Wang and Lou (1990) also developed several forms of fatigue damage laws in the framework of damage mechanics.

Generally, fatigue experimental results are presented in terms of the Paris' law in fracture mechanics and with the $S - N$ curve in damage mechanics, whereas both are merely phenomenological interpretation of the material degradation. Understanding the implicit connection between the fatigue response and the parameters describing the material degradation at the corresponding scales would permit to develop generalized models regardless of materials.

The *cohesive crack model* (Carpinteri 1985) has been widely applied to characterize the behavior of an interface under monotonic loading, with some recent applications to cyclic loading. Different shapes of the traction-relative displacements relation have been proposed. Polynomial and exponential types were used to model particle debonding and interfacial void nucleation (Needleman 1990a,b; Xu and Needleman 1993). Recently, there are some attempts to employ this model in fatigue problems by coupling damage or irreversible energy dissipation. de-Andrés et al. (1999) introduced a damage parameter into the cohesive crack model. Nguyen et al. (2001) considered the unloading-reloading hysteresis in the cohesive law to capture the dissipation under cyclic load. Yang et al. (2001) proposed to insert the internal singular surface into the quasi-brittle bulk material to take fatigue damage into account. Roe and Siegmund (2003) established an irreversible cohesive law for interface fatigue problems, which was subsequently extended by Bouvard et al. (2009) to creep-fatigue crack growth. Maiti and Geubelle (2005, 2006) also implemented a cohesive crack model to capture the crack retardation phenomenon in polymer.

Although fatigue experiments in polymers (Hertzberg 1995) have shown a relatively shorter crack initiation phase and higher sensitivity to loading levels as compared to metals, the existence of the crazing zone (a network of fine cracks) at the crack tip in fracturing polymers is analogous to the cohesive zone in metals and concretes. Thus, the cohesive crack model seems to be reasonable to describe the fracture responses of adhesive polymers in the interfaces (Maiti and Geubelle 2005, 2006). In this paper, we propose an analytical model for fatigue based on damage mechanics and cohesive crack model, inspired by the pioneering approach by Roe and Siegmund (2003). We focus our attention on a double cantilever beam (DCB), where two metallic substrates are bonded together by a polymeric adhesive. Furthermore, an analytical approach based on a beam on an elastic foundation, as formerly proposed by Williams and Hadavinia (2002) for monotonic loading and subsequently generalized by Carpinteri et al. (2008) in case of a periodic distribution of microdefects along the interface, is here extended to cyclic loading. The evolution of fatigue damage is taken into account by considering an average opening displacement of the cohesive zone length. The effects of the parameters entering the damage evolution law on crack initiation and propagation are analytically quantified. In addition, we investigate the correlation between the Paris' and Wöhler curves and the parameters of the damage model, trying to determine the relation between the evolution of damage along the interface and the global mechanical response.

2 Mathematical formulation

The basic assumption of the cohesive crack model (Carpinteri 1985; Carpinteri et al. 1985) is the formation, as an extension of the real crack, of a fictitious crack, referred to as the process zone, where the material, albeit damaged, is still able to transfer stresses. The point separating the stress-free area, i.e., the real crack, from the process zone, is called real crack tip, whilst the point separating the process zone from the undamaged material is referred to as fictitious crack tip. The process zone represents the region where energy dissipation takes place: it begins to form when the principal tensile stress reaches the material ultimate tensile strength, σ_u, and it propagates in the direction perpendicular to the direction of the principal tensile stress. Since an interface already exists, this is usually the weakest link and the present work thus assumes the interface as the crack path *a priori*. Furthermore, in the process zone, the tractions are functions of the displacement discontinuity, according to the specified cohesive law.

The interfacial traction-separation behavior is characterized by a linear softening relationship (Elices et al. 2000; Suo et al. 1992) as shown Fig. 1, where the real

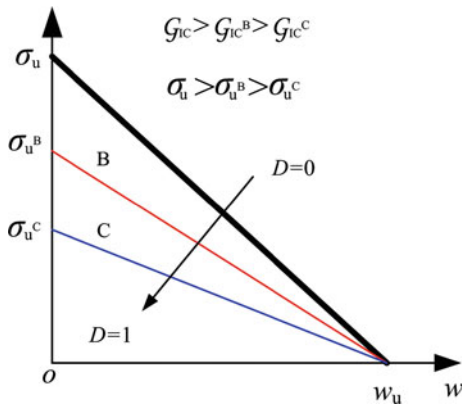

Fig. 1 The shape of the linear-softening cohesive law

crack tip corresponds to the point where the distance between the crack surfaces is equal to the critical opening displacement, w_u. The cohesive tractions are computed as follows:

$$\sigma = \sigma_u \left(1 - \frac{w}{w_u}\right). \tag{1}$$

The interface fracture energy $\mathcal{G}_{IC}$ is given by the area under the $\sigma - w$ diagram:

$$\mathcal{G}_{IC} = \int_0^{w_u} \sigma \, dw = \frac{1}{2}\sigma_u w_u, \tag{2}$$

so that the slope of the traction–displacement law is:

$$k_0 = -\frac{\sigma_u^2}{2\mathcal{G}_{IC}} = -\frac{2\mathcal{G}_{IC}}{w_u^2}. \tag{3}$$

The double cantilever beam test is widely adopted for the study of interface fracture, and a scheme of the adhesive bonded DCB specimen investigated in this study is shown in Fig. 2a. Neglecting the effect of shear deformation and damage, the vertical displacements along the interface can be determined according to the well-known Euler–Bernoulli beam theory:

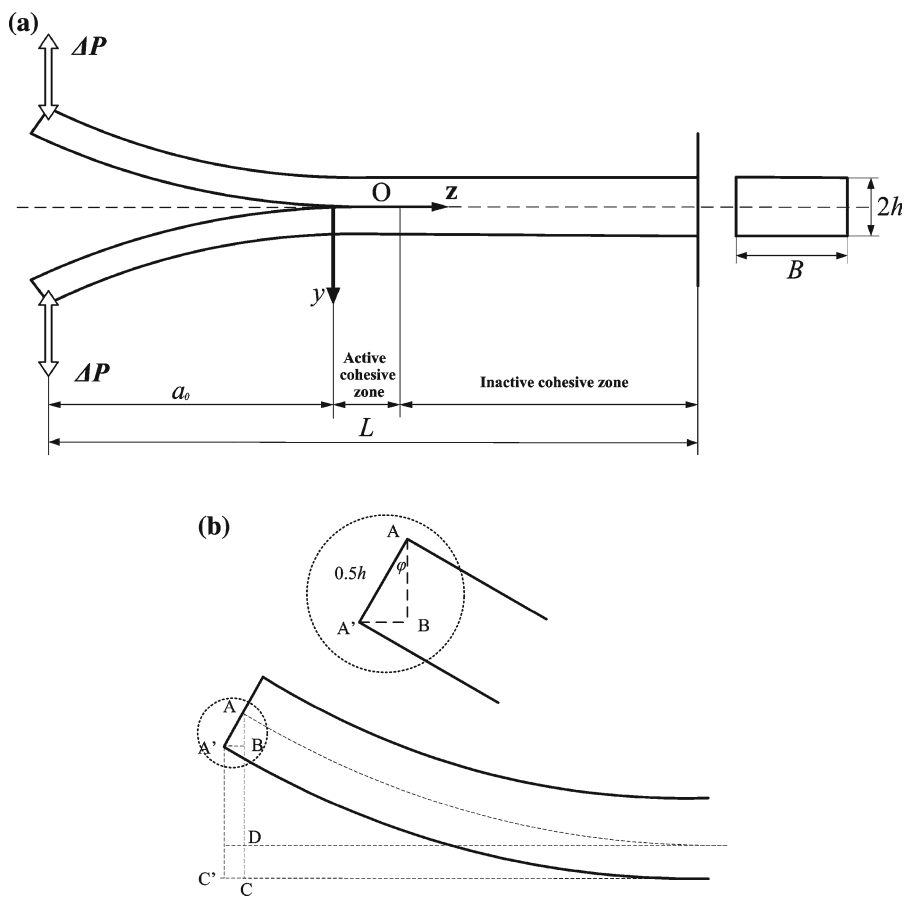

Fig. 2 Scheme of a DCB with a initial crack under cyclic load (**a**) and measurement of CMOD (**b**)

$$\frac{\mathrm{d}^4 w}{\mathrm{d}z^4} = \frac{q}{EI} = \frac{B\sigma_{\mathrm{u}}^2}{2EI\mathcal{G}_{\mathrm{IC}}}(w_{\mathrm{u}} - w) = \frac{4}{\Delta^4}(w_{\mathrm{u}} - w), \tag{4}$$

where

$$\Delta = \left(\frac{8EI\mathcal{G}_{\mathrm{IC}}}{B\sigma_{\mathrm{u}}^2}\right)^{\frac{1}{4}} = \left(\frac{2EIw_{\mathrm{u}}^2}{B\mathcal{G}_{\mathrm{IC}}}\right)^{\frac{1}{4}}. \tag{5}$$

The parameter Δ has the dimension of a length and represents a characteristic length of deformation zone. In the present context, the distributed load is given by the cohesive tractions multiplied by the thickness of the beam, $q = -B\sigma$. Here, E is the elastic modulus, I is the second moment of inertia of the beam cross-section, B is the beam thickness and z is the coordinate along the interface originating at the real crack tip (see Fig. 2a).

The general solution of Eq. (4) is:

$$w = w_0 + K_1 \sinh\sqrt{2}\frac{z}{\Delta} + K_2 \cosh\sqrt{2}\frac{z}{\Delta} + K_3 \sin\sqrt{2}\frac{z}{\Delta} + K_4 \cos\sqrt{2}\frac{z}{\Delta}, \tag{6}$$

where K_1, K_2, K_3 and K_4 are the coefficients to be determined by the boundary conditions. Beam rotation, ϕ, bending moment, M, and shear force, T, can be obtained through differentiation of w. At the real crack tip ($z = 0$), $\mathrm{d}^2w/\mathrm{d}z^2 = Pa/EI$, $\mathrm{d}^3w/\mathrm{d}z^3 = P/EI$; at the fictitious crack tip ($z = l$), $w(l) = 0$, $M(l) = 0$, $\varphi(l) = 0$. Therefore, the following result is provided:

$$w = w_0 + f_1(P)\sinh\sqrt{2}\frac{z}{\Delta} + \frac{Pa\Delta^2}{4EI}\cosh\sqrt{2}\frac{z}{\Delta} + f_2(P)\sin\sqrt{2}\frac{z}{\Delta} - \frac{Pa\Delta^2}{4EI}\cos\sqrt{2}\frac{z}{\Delta}, \tag{7}$$

where

$$f_1(P) = -Pa\Delta^2\left(\sinh\sqrt{2}\frac{l}{\Delta} + \sin\sqrt{2}\frac{l}{\Delta} - \sqrt{2}\frac{\Delta}{a}\cos\sqrt{2}\frac{l}{\Delta}\right)/4EI \times \left(\cosh\sqrt{2}\frac{l}{\Delta} + \cos\sqrt{2}\frac{l}{\Delta}\right), \tag{8a}$$

$$f_2(P) = f_1(P) - \frac{P\Delta^3}{\sqrt{2}EI}. \tag{8b}$$

The opening displacements of the beam for $z > 0$ are these of a classical beam on an elastic foundation, which have both negative and positive signs. When the displacement is negative, interpenetration along the interface occurs. The contact constraints are not enforced in this study due to its negligible effect in absence of pre-existing defects (Carpinteri et al. 2008), and special emphasis is given to the positive (opening) displacements along the interface of the DCB, i.e., the active process zone.

The thickness of the beam might affect the estimation of the CMOD, which is estimated as 2×AD in Fig. 1b, whereas its exact value is equal to $2 \times A'C'$. Thus, the relative error in the estimation of the CMOD is given by: Error $= \frac{\mathrm{A'C'-AD}}{\mathrm{AD}} = \frac{\mathrm{CD-AB}}{\mathrm{AD}} = \frac{1}{2}\frac{h}{\mathrm{AD}}(1 - \cos\phi)$.

In addition, the ratio between Δ and h in equation (4) is highly related to the shear effect. Thus, regarding the examples analyzed here, to be considered ($\mathcal{G}_{\mathrm{IC}} = 550\mathrm{N/m}$), the size of the fully developed process zone is about 43.76 mm, which is approximately three times the beam depth h. Accordingly, φ is relatively small (<1°), and the estimated value of CMOD is accurate enough in the present case. However, Eq. (4) can also be formulated according the Timoshenko beam theory to capture shear deformation effects (Williams and Hadavinia 2002), and the present calculation gives a relative error of 3.7% in the length of process zone. Therefore, the Euler–Bernoulli beam model is appropriate for the present cases.

The cohesive constitutive law has to be coupled with damage in order to capture finite life effects. Therefore, the increment of damage is related to the increment of deformation and weighted by the current load level, as proposed by Lemaitre (1996) and numerically confirmed by Roe and Siegmund (2003). The model is based on these assumptions in accordance to the nonlinear continuous damage theory by Chaboche (1988a,b). Here, a damage variable D is introduced to quantify the increasing degradation of the interface properties under cyclic loading. This state-dependent cohesive model has been used to capture the interface fatigue failure events by Roe and Siegmund (2003) and Maiti and Geubelle (2005). The irreversible mechanical dissipation must be non-negative to satisfy energetic requirements, i.e., $\Delta D \geq 0$. Usually, D increases monotonically from zero (infinite fatigue life or reversible dissipation) to unity (occurrence of a macro-crack). During unloading, the accumulated damage is maintained until forthcoming reloading, and no healing takes place. Therefore, D is a macroscopic parameter used to capture the loss of integrity due to microscopic chemical bond breakages in the cohesive zone, at the front of the macrocrack tip. The irreversible

accumulated damage D_N after N cycles gives to the progressive reduction of the cohesive energy $\mathcal{G}_{\mathrm{IC}}$, the cohesive stiffness k and the cohesive strength σ_{u} from the initial values, as shown in Fig. 1. These cohesive properties are gradually degraded until final failure at $D = 1$. The instantaneous cohesive parameters are:

$$\mathcal{G}_{N+1} = \mathcal{G}_{\mathrm{IC}}(1 - D_N), \tag{9a}$$

$$k_{N+1} = k_0(1 - D_N), \tag{9b}$$

$$\sigma_{\mathrm{uN+1}} = \sigma_{\mathrm{u}}(1 - D_N), \tag{9c}$$

where $\mathcal{G}_{\mathrm{IC}}$, k_0 and σ_{u} denote the initial critical values, whereas $\mathcal{G}_{N+1}$, k_{N+1}, $\sigma_{\mathrm{u}N+1}$ are the updated ones after N cycles. Naturally, $D = 1$ is defined as the crack extension criterion. Equations (9) indicate that the constitutive cohesive law is coupled with the damage accumulation by substituting the initial cohesive crack law parameters with the current ones.

As a result, introducing Eq. (9a) (or damage variable) into the previous analytical beam model, Eq. (4), the damage-dependent crack opening displacement is:

$$w_D = w_0 + f_1(P)\sinh\sqrt{2}\frac{z}{\Delta_D} + \frac{Pa\Delta_D^2}{4EI}\cosh\sqrt{2}\frac{z}{\Delta_D} + f_2(P)\sin\sqrt{2}\frac{z}{\Delta_D} - \frac{Pa\Delta_D^2}{4EI}\cos\sqrt{2}\frac{z}{\Delta_D}, \tag{10}$$

where

$$\Delta_D = \left(\frac{2EIw_{\mathrm{u}}^2}{BG_{\mathrm{IC}}(1-D)}\right)^{\frac{1}{4}}, \tag{11a}$$

and

$$f_1(P) = -Pa\Delta_D^2\left(\sinh\sqrt{2}\frac{l}{\Delta_D} + \sin\sqrt{2}\frac{l}{\Delta_D} - \sqrt{2}\frac{\Delta_D}{a}\cos\sqrt{2}\frac{l}{\Delta_D}\right)\Big/ 4EI\left(\cosh\sqrt{2}\frac{l}{\Delta_D} + \cos\sqrt{2}\frac{l}{\Delta_D}\right), \tag{11b}$$

$$f_2(P) = f_1(P) - \frac{P\Delta_D^3}{\sqrt{2}EI}. \tag{11c}$$

As indicated by Eqs. (10) and (11), the crack opening displacement w_D permits to describe mechanical degradation in terms of the load level P and current damage status D. In other words, the opening displacement, w_D, is a function of the damage level and the beam coordinate, z, or, in non-dimensional form, z/Δ_D. According to Eqs. (10) and (11), the interface opening displacement from $z = 0$ to the real crack tip can be computed and it is schematically shown in Fig. 3. It is in the active cohesive zone that the complex damage phenomena take place, which are associated to crazing and/or discontinuous crack growth. Furthermore, the increment of damage is associated to the deformation in the active process zone, weighted by the current load level and cohesive properties (Lemaitre 1996).

Deformation damage variable is crucial to describe the fatigue damage process in conjunction with the cohesive crack model. In principle, different expressions could be considered, as reviewed by Chaboche (1988a,b) and Krajcinovich (1984). Specifically, effective parameters in damage mechanics have been widely applied (Lemaitre 1996): only part of the material can withstand the load due to the presence of micro-discontinuities. In this context, the damage variable is efficiently defined through the ratio between the sum of the areas of the micro-discontinuities and the original undamaged area. In our work, due to a traction–separation law as the constitutive law for the interface, the cohesive tractions are directly related to the deformation, that is, the opening displacement. Similarly, the effective opening displacement (or deformation) is assumed to be representative of the area where the nonlocal degradation of the process zone due to micro-discontinuities takes place. Consequently, damage is related to the opening displacement in the active process zone, and its evolution is formulated as follows:

$$D_{N+1} = D_N + \left[\alpha\frac{w_{effe}}{w_{\mathrm{u}}}\right]^{\gamma}, \tag{12}$$

where $w_{effe} = \frac{w_{N+1}^{ave}}{(1-D_N)}$ is the effective opening displacement after $(N+1)$ cycles, and D_N is the amount of accumulated damage after N cycles. Moreover, the average opening displacement w_{N+1}^{ave} for the $(N+1)$th cycle is defined as follows:

$$w_{N+1}^{ave} = \frac{\int_0^{l_{cz}} w_{D_N} dz}{l_{cz}}, \tag{13}$$

where w_{D_N} is given in Eq. (10) with the corresponding damage D_N. More specifically, the increment of damage is evaluated as the ratio between the effective opening displacement w_{effe} and the initial critical opening displacement w_{u} (see Fig. 1) multiplied by a coefficient α and raised to power γ. In Eq. (12), α and γ are material parameters. Hence, the opening displacement increases linearly with the applied load P. Moreover, since the displacement enters Eq. (12) and is raised to a power γ, this results into a nonlinear dependency between damage increment and load

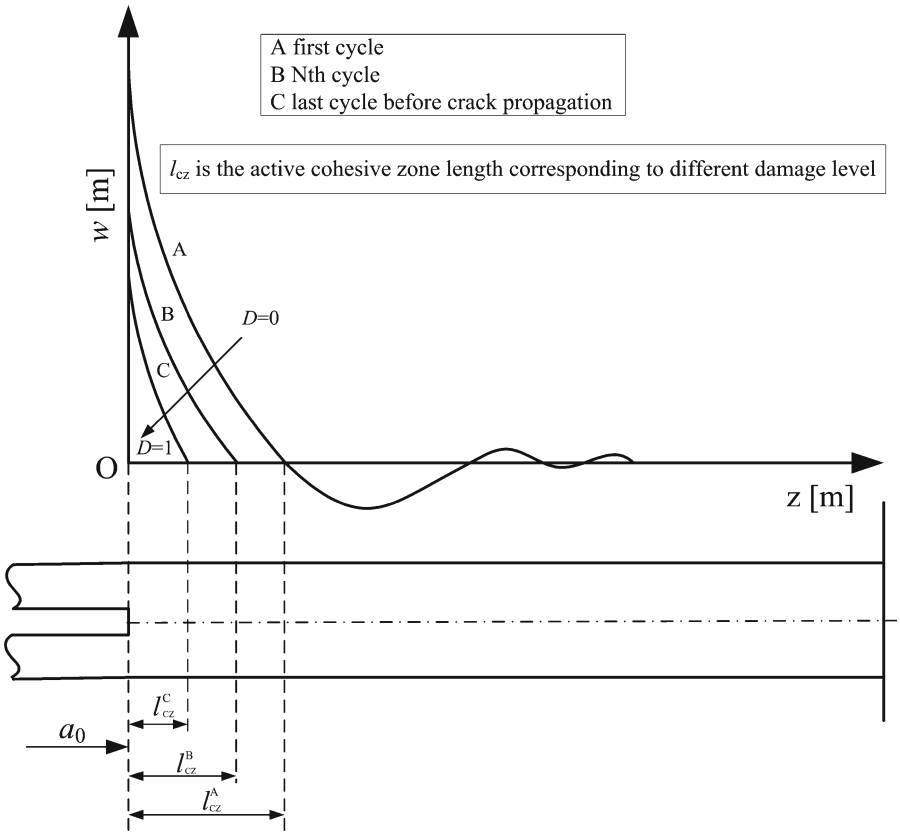

Fig. 3 Crack opening displacement along the interface at $z > 0$ at different damage levels

level. A similar nonlinear dependency on the load level was present in by Roe and Siegmund (2003). During each cyclic load, the cohesive properties of the active process zone gradually reduce as the opening displacement increases. Therefore, the damage evolution law in Eq. (12) is able to take both the deformation/load level (Eq. 10) and its history into account, which is a general representation of the complex damage and fracture phenomena in the process zone (Lemaitre 1996).

Furthermore, the effect of different damage levels on the interface cohesive response is quantitatively depicted in Figs. 3 and 4. The curve A corresponds to the first cycle with no damage, $D_A = 0$, and the curve B is at a certain level of damage, $D_B > 0$. The curve C represents the maximum level of damage leading to crack propagation. It is worth mentioning that the ultimate load diminishes gradually when D approaches unity (macro-crack formation). Meanwhile, the opening displacements along the interface of the DCB for $z > 0$ vary with the damage level, and it gives rise to the P vs. CMOD relationship in Fig. 4. The degradation leads to the reductions of the stiffness and

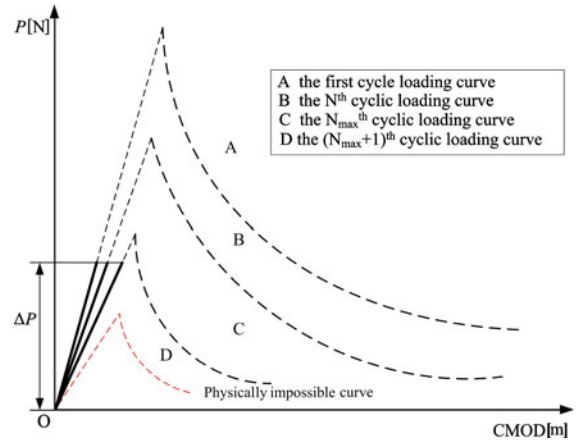

Fig. 4 Typical ΔP versus CMOD curves of DCB for different levels of damage

the ultimate strength. When the damage variable D is equal to unity, crack initiation takes place. Similar with the plastic zone at the crack tip of metals, the crack in polymer propagates in the form of crazing. Due to

the accumulation of damage ahead of the fatigue crack over certain cycles, the failure of fibrils in the process zone may lead to the crack jump suddenly through the crazing zone length (Skibo et al. 1977). Accordingly, to characterize fatigue crack propagation, we prescribe the amount of crack extension not infinitesimal but of finite value when the critical damage level is reached, which is fully consistent with the finite fracture mechanics approaches by Leguillon (2002) and Taylor et al. (2005). According to the fracture criterion by finite fracture mechanics (Cornetti et al. 2006), the crack increment is set equal to the initial active cohesive zone length, l_{cz}^{A}.

3 The effect of damage evolution on crack initiation

The model proposed in the previous section is applied here to predict crack initiation. As a case study, the following geometrical and mechanical parameters of the DCB test are considered: $a_0 = 30\,\text{mm}$, $l = 100\,\text{mm}$, $h = 5\,\text{mm}$, $B = 20\,\text{mm}$, $E = 69\,\text{GPa}$, $\sigma_u = 57\,\text{MPa}$, $\mathcal{G}_{IC} = 5\text{kJ/m}^2$. In this simulation, γ and α are set as 3.5 and 4.0, respectively. Considering an applied cyclic load of $\Delta P = 450\,\text{N}$ with the loading ratio $R = 0$, the analytical P vs. CMOD responses and the interface displacements are shown in Figs. 5 and 6, respectively. As expected, with ongoing cycles, the accumulated damage increases and results into a gradual reduction of interface fracture toughness and maximum strength (the cyclic load is denoted by a red line). As the damage increases until the final cycle corresponding to the onset of crack growth, $D = 1$, the maximum load becomes lower than the applied cyclic load P_{max} (see Fig. 4). Additionally, Fig. 7 represents the damage evolution vs. cycle for different loading levels. For a larger number of cycles the rate of damage accumulation is also higher, especially when the damage value approaches 0.7. These phenomena are in qualitative agreement with the experimental results in Chaboche and Lesne (1988).

The number of cycles required for crack initiation are calculated for different loading levels and the results are interpreted in terms of Wöhler or $S - N$ curves $\Delta P = W \times N^{\beta}$, where W and β are Wöhler parameters (see Figs. 8, 9). Here, N denotes the predicted number of cycles for crack initiation. The obtained global ΔP vs. N curves required for crack initiation for different values of γ and α are shown in Figs. 8 and 9, respectively. It is interesting to note that the proposed cohesive crack model combined with damage mechanics correctly provides power-law relations in the ΔP vs.

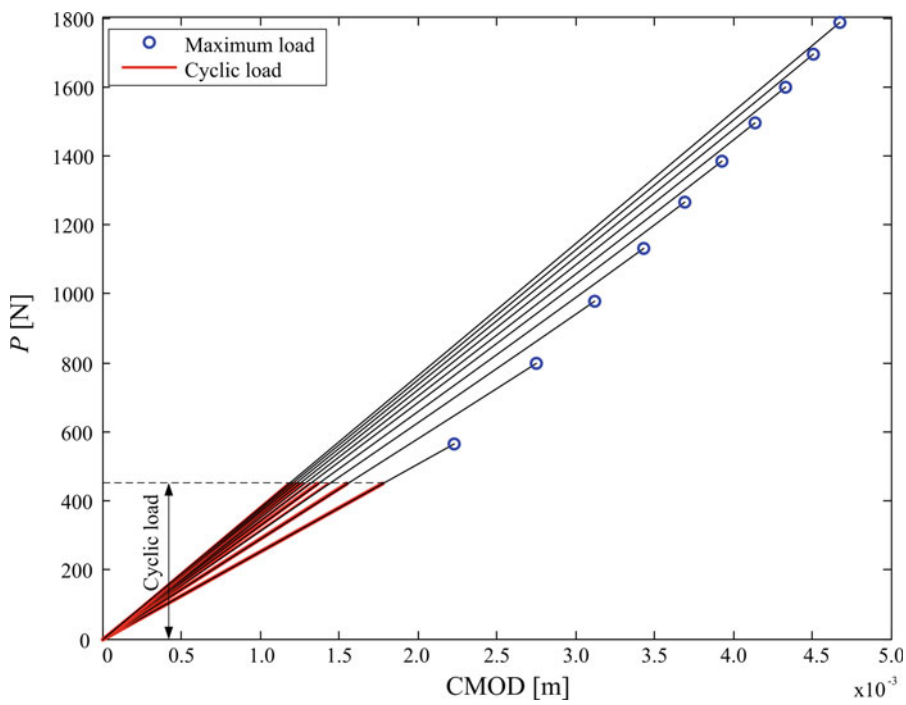

Fig. 5 ΔP versus CMOD curves for DCB with damage accumulation until crack initiation ($\Delta P = 450\,\text{N}$, $\gamma = 3.5$, $\alpha = 4.0$ and $a_0 = 30\,\text{mm}$)

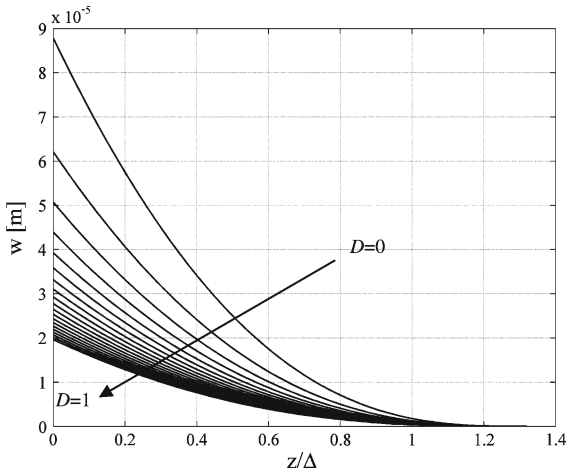

Fig. 6 Crack opening displacement along the interface as damage evolution ($\Delta P = 450\,\text{N}, \gamma = 3.5, \alpha = 4.0$ and $a_0 = 30\,\text{mm}$)

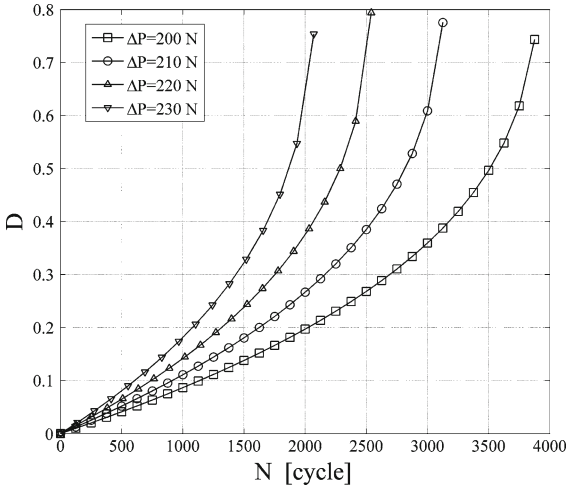

Fig. 7 Damage evolution predicted by the model with linear-softening cohesive law ($\gamma = 3.5, \alpha = 4.0$ and $a_0 = 30\,\text{mm}$)

N plane, which is an indirect confirmation of the effectiveness of the proposed model. From Fig. 8 we note that the curves have the same intercept with the vertical axis and that the slope β is remarkably dependent on γ, i.e., it is approximately equal to $-1/\gamma$. As a confirmation, the coefficient β does not change if γ is kept constant (see Fig. 9). On the other hand, the parameter α shifts the $S - N$ curves.

4 The effect of damage evolution on crack propagation

Paris's law originally used for metals is also applicable to many polymers, although the material properties are

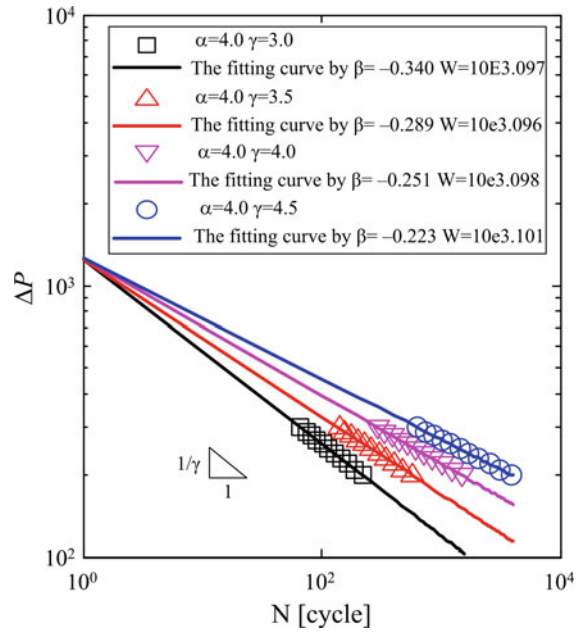

Fig. 8 Effect of γ on the $S - N$ curves of crack initiation ($\alpha = 4.0$ and $a_0 = 30\,\text{mm}$)

quite different. For instance, the exponent m of Paris' equation is about 6, whereas it is approximately equal to 3 in metals, suggesting that crack propagation in polymers is a faster process (Hertzberg 1995). Thus, one of the primary aims in polymer fatigue is to measure the fatigue crack growth rate (FCGR), $\mathrm{d}a/\mathrm{d}N$, and relate it to fracture mechanics parameters, such as the strain energy release rate $\mathcal{G}$ or stress-intensity factor K. For instance, the former is usually the preferred fracture parameter in bonded components with interfaces. Hence, There are three regions generally recognized in the $\mathrm{d}a/\mathrm{d}N$ vs. $\Delta\mathcal{G}$ diagram. Region I is the near-threshold region without crack propagation. In Region II, there exists a power-law relationship between crack growth rate and $\Delta\mathcal{G}$. Finally, rapid crack propagation and growth instability take place in Region III.

Here, the same geometric and mechanical parameters used in Sect. 3 are adopted. The results in terms of $\mathrm{d}a/\mathrm{d}N$ vs. $\Delta\mathcal{G}$ are obtained using the model derived in Sect. 2. Since many polymers present crack jumps or discontinuous crack growth under tension (Skibo et al. 1977; Hertzberg 1995), the discrete crack increment is assumed to be $\Delta a = l_{\mathrm{cz}}^{\mathrm{A}}$. The effects of α and γ are shown in Figs. 10 and 11, and fitted by a power-law,

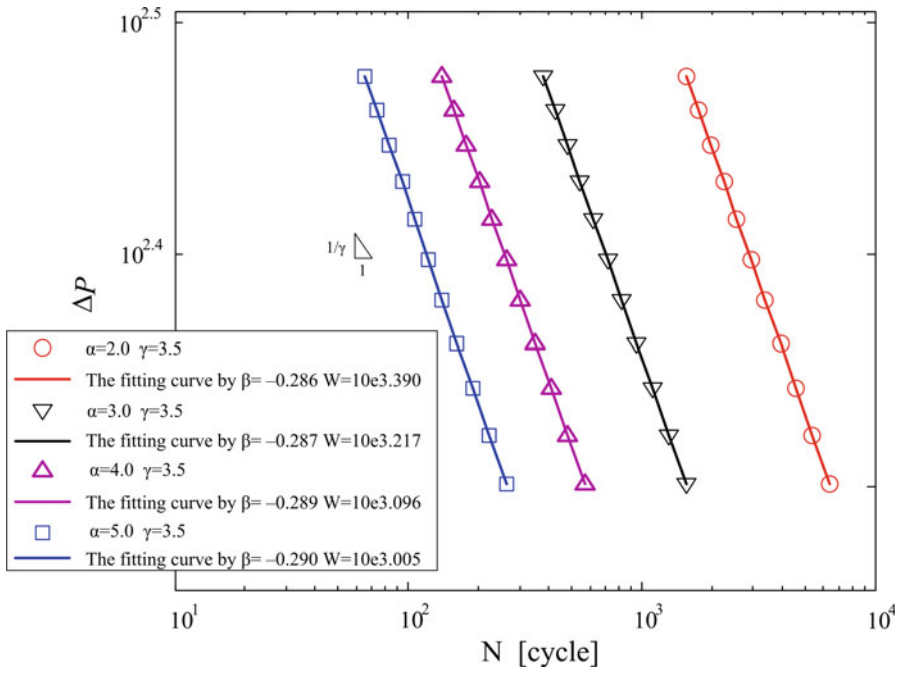

Fig. 9 Effect of α on the $S-N$ curves of crack initiation ($\gamma = 3.5$ and $a_0 = 30\,\text{mm}$)

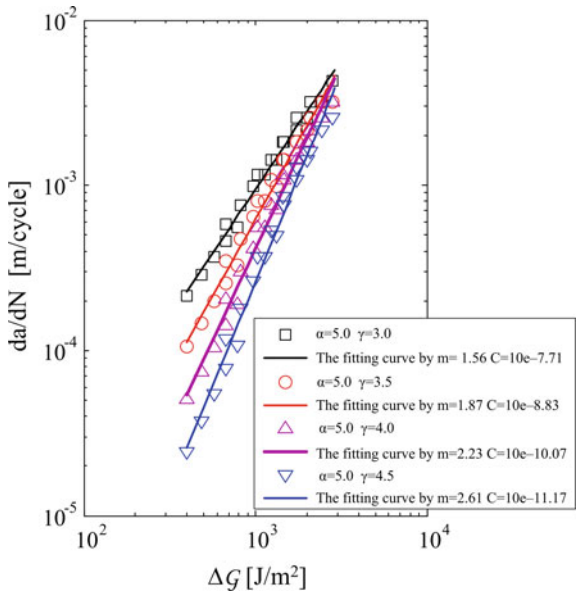

Fig. 10 Predicted relationship between FCGR and applied energy release rate range for different values of γ

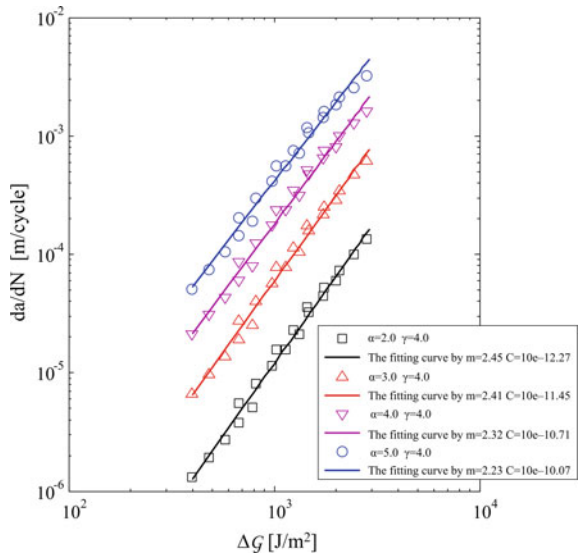

Fig. 11 Predicted relationship between FCGR and applied energy release rate range for different values of α

$\mathrm{d}a/\mathrm{d}N = C(\Delta\mathcal{G})^m$, where the applied strain energy release rate range is $\Delta\mathcal{G} = (\mathcal{G}_{\max} - \mathcal{G}_{\min})$. For the DCB investigated here, the Mode I strain energy release rate range under the applied load range ΔP is (ASTM G168):

$$\Delta\mathcal{G} = \frac{12(\Delta P)^2 a^2}{B^2 h^3 E}. \tag{14}$$

As illustrated in Fig. 10, the parameter γ has a significant influence on the damage accumulation, leading to very different slopes of the $\mathrm{d}a/\mathrm{d}N$ vs. $\Delta\mathcal{G}$ curves. Keeping γ constant, the effect of the parameter α on

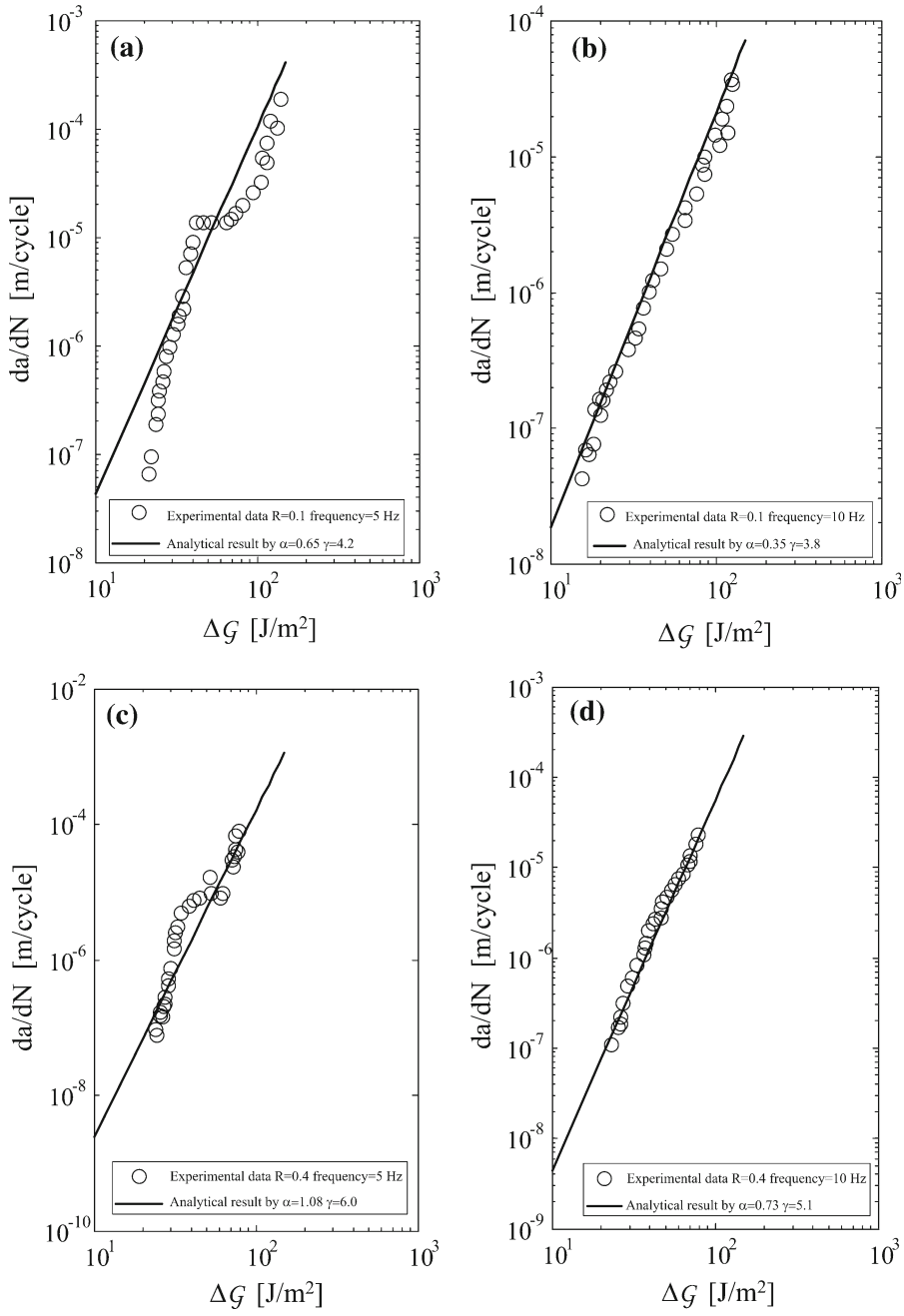

Fig. 12 Comparison of analytical and experimental results adopted from Pirondi and Nicoletto (2004) in terms of FCGR and applied energy release rate

the Paris' curves is investigated in Fig. 11: the higher the parameter α, the lower the intercept C.

5 Comparison with fatigue experiments

To propose an experimental assessment of our model, a DCB test with aluminum alloy beams bonded by Multi-bond 330 tested by Pirondi and Nicoletto (2004) is considered. The mechanical properties of the bulk adhesive are $E = 70\,\text{GPa}$, $\sigma_u = 8.6\,\text{MPa}$, $\mathcal{G}_{IC} = 550\text{N/m}$. The geometrical parameters are $a_0 = 40\,\text{mm}$, $l = 120\,\text{mm}$, $h = 15\,\text{mm}$, $B = 30\,\text{mm}$. Analytical predictions are compared with experimental $\text{d}a/\text{d}N$ vs. $\Delta\mathcal{G}$ results at different frequencies and loading ratios R in Fig. 12. The best-fitting Paris' law parameters for both

Table 1 The comparison between the experiments and analytical predictions

$da/dN = C(\Delta\mathcal{G})^m$		Analytical parameters		Analytical predictions		Experiments	
Frequency	R	α	γ	m	C	m	C
5 Hz	0.1	0.65	4.2	3.382	$10^{-10.757}$ [$m^{7.764}$/(cycle·$J^{3.382}$)]	3.370	$10^{-10.890}$ [$m^{7.740}$/(cycle·$J^{3.370}$)]
	0.4	1.08	6.0	4.810	$10^{-13.412}$ [$m^{10.620}$/(cycle·$J^{4.810}$)]	4.863	$10^{-13.405}$[$m^{10.726}$/(cycle·$J^{4.863}$)]
10 Hz	0.1	0.35	3.8	3.050	$10^{-10.781}$[$m^{7.100}$/(cycle·$J^{3.050}$)]	2.910	$10^{-10.702}$[$m^{7.764}$/(cycle·$J^{3.382}$)]
	0.4	0.73	5.1	4.102	$10^{-12.440}$[$m^{9.204}$/(cycle·$J^{4.102}$)]	4.115	$10^{-12.420}$[$m^{9.230}$/(cycle·$J^{4.115}$)]

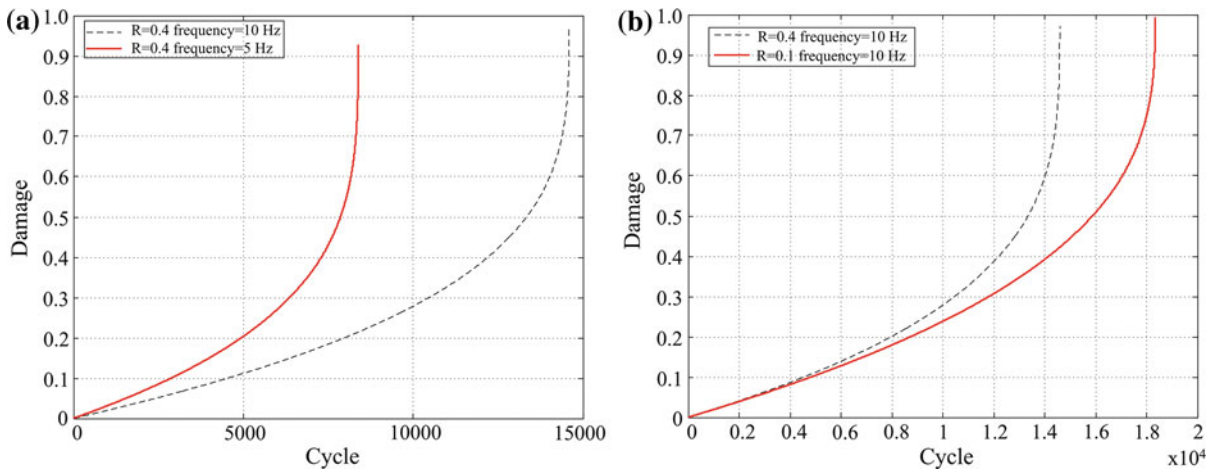

Fig. 13 The effects of frequency (**a**) and load ratio (**b**) on damage accumulation rate

experiments and predictions are listed in Table 1. The proposed fatigue cohesive crack model can capture the power-law region very well as shown in Fig. 12. The influences of frequency and loading ratio are two important aspects affecting crack growth rate of polymers.

In addition, the damage evolution related to the effects of frequency and loading ratio are depicted in Fig. 13, where the results under four combinations of frequency and loading ratio, $R = 0.1$ and 0.4 at frequency 10 Hz and frequencies 5 and 10 Hz, are compared. In Fig. 13a, we note the pronounced decrease of damage accumulation rate with a higher cyclic frequency, which can be appreciated by comparing the slope of damage evolution curves. Similar frequency sensitivity in some polymers has been reported in the review by Hertzberg (1995). More in details, according to Pirondi and Nicoletto (2004), the loading frequency effect on fatigue crack growth rate of adhesive can be attributed to temperature effects. In other words, an increase of the loading frequency results into a non-proportional increase of the temperature at the crack tip, which may alter the polymer properties. Furthermore, heating effect leads to a lower stiffness consistent with our Eq. (9b). The effect of loading ratio is illustrated in Fig. 13b, where we observe that the

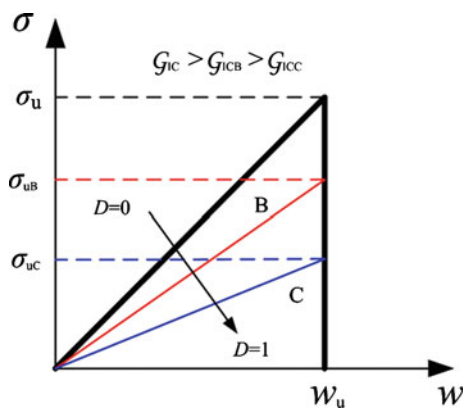

Fig. 14 Tension cut-off cohesive constitutive law with different damage levels

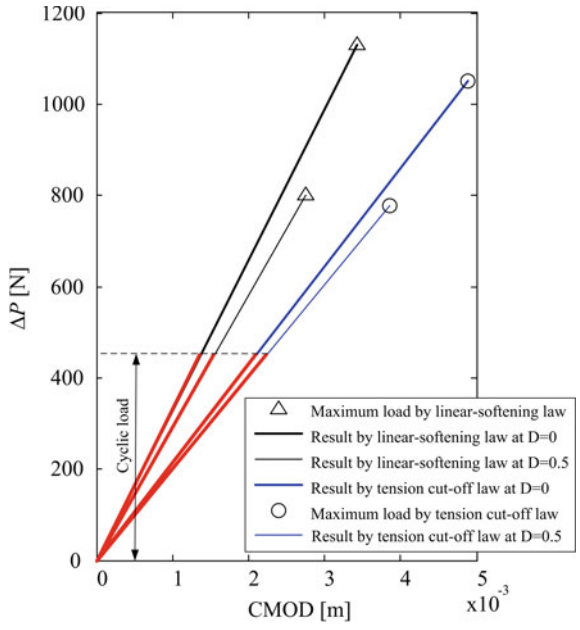

Fig. 15 ΔP versus CMOD curves for different cohesive laws and damage levels

damage rate is an increasing function of R. In addition, load amplitude ΔP was varied during the fatigue tests so as to introduce different strain energy release rate range, $\Delta\mathcal{G}$. This is the reason why different sets of parameters α and γ were required to fit the experimental data by Pirondi and Nicoletto (2004). In principle, tests performed under constant load amplitude and different loading ratios should be fitted using the same model parameters.

6 Effect of the shape of cohesive crack law

In this section, to assess the effect of the shape of the cohesive crack law on the fatigue performance, we consider a tension cut-off traction–displacement relation for the interface shown in Fig. 14 and given by the following equation:

$$\sigma = k_0(1-D)w = \frac{2\mathcal{G}_{\mathrm{IC}}(1-D)}{w_{\mathrm{u}}^2}w. \tag{15}$$

The area under the traction–displacement is also interpreted as the interface fracture energy $\mathcal{G}_{\mathrm{IC}}$. The analytical predictions using tension cut-off and the linear-softening forms are compared in terms of the ΔP vs. CMOD curves in Fig. 15. Both the maximum load for crack initiation under monotonic loading and the stiffness of the composite beam are different. More specifically, the cohesive crack model with a linear-softening shape leads to a stiffer behavior and to a higher maximum load as compared to that with the tension cut-off shape. As the accumulated damage increases (see the curve with $D = 0.5$ in Fig. 15), the maximum load and the stiffness of DCB decrease gradually, but the reduction in stiffness predicted by the linear-softening law is more pronounced. Furthermore, the $S-N$ curves for the cohesive crack model with the

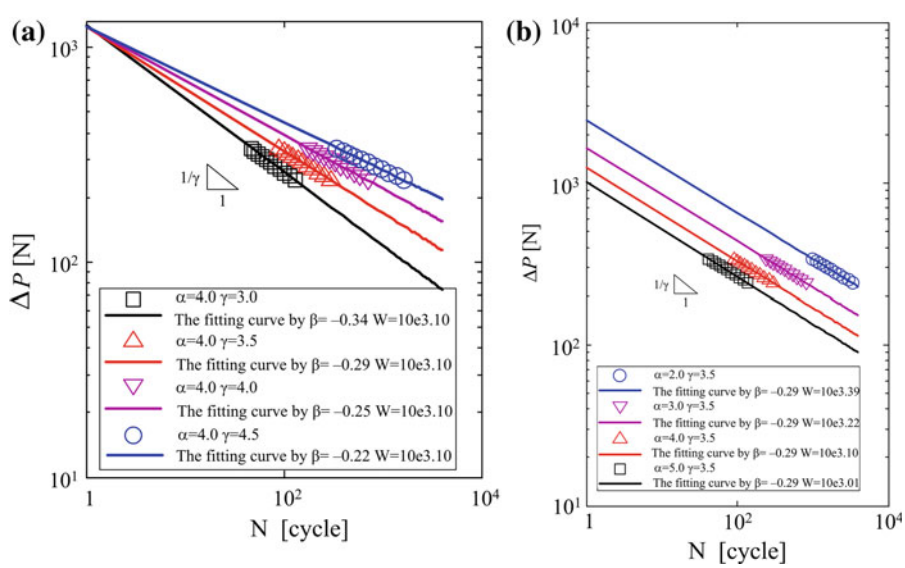

Fig. 16 Effect of γ on the $S-N$ curves of crack initiation ($\alpha = 4.0$ and $a_0 = 30\,\mathrm{mm}$) (**a**); effect of the parameter α on the $S-N$ curves of crack initiation ($\gamma = 3.5$ and $a_0 = 30\,\mathrm{mm}$) (**b**)

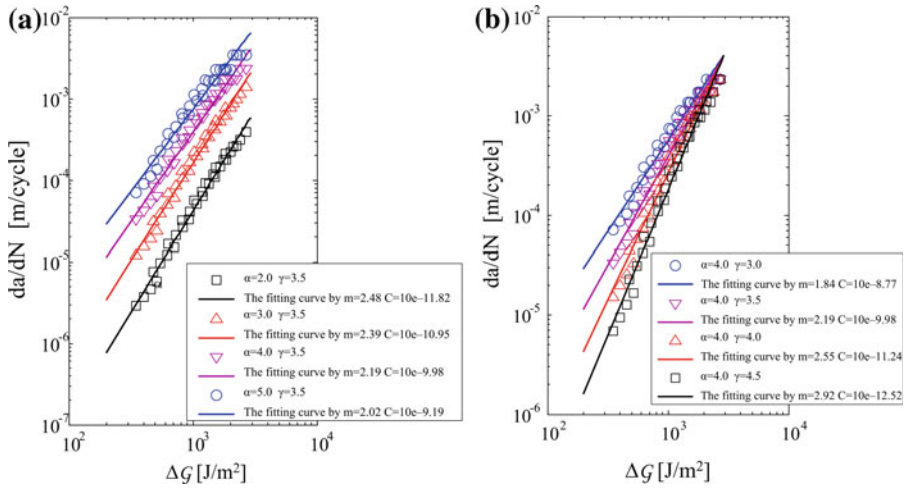

Fig. 17 Predicted relationship between FCGR and applied energy release rate range for different values of α (**a**); Predicted relationship between FCGR and applied energy release rate range for different values of γ (**b**)

tension cut-off shape are shown in Fig. 16 by varying the parameters α and γ, respectively. Also, in this case, slope of the $S-N$ curves is approximately equal to $-1/\gamma$. The same discontinuous crack propagation assumption is implemented to obtain the $\mathrm{d}a/\mathrm{d}N$ vs. $\Delta\mathcal{G}$ curves shown in Fig. 17. Compared with Sect. 4, it appears that the effects of the parameters α and γ in both cases are identical, and the roles of these parameters are thus independent of the chosen cohesive crack law.

7 Conclusions

In this paper, the cohesive crack model has been used to describe the fatigue response of a DCB. To capture finite life effects, the model considers a constitutive cohesive traction–displacement relation coupled with damage. Hence, a damage mechanics formulation has been employed to quantify the damage rate due to cyclic loading. Accordingly, the evolution of damage with the number of load cycles was prescribed explicitly in the model. More specifically, damage is related to the deformation in the active process zone, weighted by the current load level, the critical opening displacement and the accumulated damage state variable. The analytical results provided by the model have been interpreted in terms of the $S-N$ and Paris' curves. During the crack initiation stage, fatigue damage accumulation is highly nonlinear. For the discontinuous crack propagation, a power-law of Paris' type is obtained. To validate the proposed model, the analytical results have been compared with experiments and a good agreement was noticed. Finally, the tension cut-off cohesive law has been considered to illustrate the effect of the shape of the cohesive crack law on the fatigue response. It has been found that the effects of parameters α and γ on the $S-N$ and Paris' curves are identical regardless of the shape of the cohesive crack laws.

References

ASTM G 168 (2000) Standard practice for making and using precracked double beam stress corrosion specimens. ASTM Annual Book of ASTM Standards, vol 03.02

Bouvard JL, Chaboche JL, Feyel F, Gallerneau F (2009) A cohesive zone model for fatigue and creep-fatigue crack growth in single crystal superalloys. Int J Fatigue 31:868–879

Carpinteri A (1985) Interpretation of the Griffith instability as a bifurcation of the global equilibrium. In: Shah S (eds) Application of fracture mechanics to cementitious composites (Proceedings of NATO advanced research workshop, Evanston, USA). Martinus Nijhoff, Dordrecht, pp 287–316

Carpinteri A, Di Tommaso A, Fanelli M (1985) Influence of material parameters and geometry on cohesive crack propagation. In: Wittmann FH (ed) Fracture toughness and fracture energy of concrete. Elsevier, Amsterdam pp 117–135

Carpinteri A, Paggi M, Zavarise G (2008) The effect of contact on the decohesion of laminated beams with multiple microcracks. Int J Solids Struct 45:129–143

Chaboche JL, Lesne PM (1988) A non-linear continuous fatigue damage model. Fatigue Fract Eng Mater Struct 11:1–7

Chaboche JL (1988) Continuum damage mechanics: part I-general concepts. J Appl Mech 55:59–64

Chaboche JL (1988) Continuum damage mechanics: part II-Damage growth, crack initiation, and crack growth. J Appl Mech 55:65–72

Cornetti P, Pugno N, Carpinteri A, Taylor D (2006) Finite fracture mechanics: a coupled stress and energy failure criterion. Eng Fract Mech 73:2021–2033

de-Andrés A, Pérez JL, Ortiz M (1999) Elastoplastic finite element analysis of three-dimensional fatigue crack growth in aluminum shafts subjected to axial loading. Int J Solids Struct 36:2231–2258

Dowling NE, Begley JA (1976) Fatigue crack growth during gross plasticity and the J-integral. ASTM STP 590:82–103

Elices M, Planas J, Guinea GV (2000) Fracture mechanics applied to concrete. In: Freutes M, Elices M, Martin-Meizoso A, Martmez-Esnaola JM (eds) Fracture mechanics: applications and challenges. ESIS publication 26. Elsevier, Amsterdam

Hertzberg RW (1995) Deformation and fracture mechanics of engineering materials. Wiley, New York

Kachanov LM (1958) On the time to failure under creep conditions. Izvestia Akademii Nauk SSSR, Otdelenie tekhnicheskich nauk 8:26–31

Krajcinovich D (1984) Continuum damage mechanics. Appl Mech Rev 37:1–6

Lemaitre J, Plumtree A (1979) Application of damage concept to predict creep-fatigue failures. ASME J Eng Mater Technol 101(3):284–292

Lemaitre J (1996) A course on damage mechanics. Springer, Berlin

Leguillon D (2002) Strength or toughness? A criterion for crack onset at a notch. Eur J Mech A/Solids 21:61–72

Maiti S, Geubelle PH (2005) A cohesive model for fatigue failure of polymers. Eng Fract Mech 72:691–708

Maiti S, Geubelle PH (2006) Cohesive modelling of fatigue crack retardation in polymers: crack closure effect. Eng Fract Mech 73:22–41

Mostovoy S, Ripling EJ (1975) Flaw tolerance of a number of commercial and experimental adhesives. Plenum Press, New York

Neumann P (1974) The geometry of slip processes at a propagating fatigue crack-II. Acta Metal 22:1167–1178

Needleman A (1990) An analysis of tensile decohesion along an interface. J Mech Phys Solids 38:289–324

Needleman A (1990) An analysis of decohesion along an imperfect interface. Int J Fract 42:21–40

Nguyen O, Repetto EA, Ortiz M, Radovitzky RA (2001) A cohesive model of fatigue crack growth. Int J Fract 110:351–369

Paris PC, Gomez MP, Anderson WP (1961) A rational analytic theory of fatigue. Trend Eng 13:9–14

Pirondi A, Nicoletto G (2004) Fatigue crack growth in bonded DCB specimens. Eng Fract Mech 71:859–871

Roe KL, Siegmund T (2003) An irreversible cohesive zone model for interface fatigue crack growth simulation. Eng Fract Mech 70:209–232

Suo Z, Bao G, Fan B (1992) Delamination R-curve phenomena due to damage. J Mech Phys Solids 40:1–16

Skibo MD, Hertzberg RW, Manson JA, Kim SL (1977) On the generality of discontinuous fatigue crack growth in glassy polymers. J Mater Sci 12:531–542

Taylor D, Cornetti P, Pugno N (2005) The fracture mechanics of finite crack extension. Eng Fract Mech 72:1021–1038

Wang J (1992) A continuum damage mechanic model for low-cycle fatigue failure of metals. Eng Fract Mech 41:437–441

Wang T, Lou Z (1990) A continuum damage model for weld heat affected lone under low cycle fatigue loading. Eng Fract Mech 37:825–829

Williams J, Hadavinia H (2002) Analytical solutions for cohesive zone models. J Mech Phys Solids 50:809–825

Xu XP, Needleman A (1993) Void nucleation by inclusion debonding in a crystal matrix. Model Simul Mater Sci Eng 1:111–132

Yang B, Mall S, Ravi-Chandar K (2001) A cohesive zone model for fatigue crack growth in quasibrittle materials. Int J Solids Struct 38:3927–3944